

Original Article

Optimizing Single Beam Data for Bathymetric Analysis

Ito Udoh¹, Akwaowo Ekpa², James Mbat³

^{1,2,3}Department of Geoinformatics and Surveying, University of Uyo, Uyo– Nigeria

Received: 03 November 2022

Revised: 06 December 2022

Accepted: 18 December 2022

Published: 31 December 2022

Abstract - Single beam echo sounding has been a reliable acoustic method for acquiring a depth of varying ranges with high accuracy, precision, and relatively low cost. Single beam data are valuable as ground truth data for many marine-based applications, project monitoring and bathymetry studies. In bathymetry mapping of part of Imo River, the cost-effectiveness of Single Beam Echo sounding data for generating three-dimensional bathymetric metrics for terrain characterization is demonstrated. Analysis of an accurate description of the riverbed is tested using two geo-statistic and deterministic interpolation methods. The gridding capability of Surfer 23 and ArcGIS 10.5 software and interpolation outputs from five interpolation techniques for the dataset are compared. Ordinary Kriging interpolation produced a more accurate digital depth model followed by an inverse multiquadric radial basis function. Fine and broad scale position bathymetry index and rugosity for the study area is produced to show the relative depth and slope of the seabed as well as the bathymetry's variability of slope and aspect. Resulting bathymetry metrics can be useful for navigational aid, hydrodynamic and ecological studies on the river. It can also serve as in situ depth data for calibrating and validating satellite-based bathymetry.

Keywords - Bathymetry position index, Bathymetric profiles, Depth derivatives, Interpolation, Single-beam data.

1. Introduction

Applying bathymetric information in conventionally diversified areas such as marine geomorphology, seabed composition study and classification, hydrodynamic models, flood management and prevention, and the derivation of bathymetric position index shows seabed rugosity, slope, aspect and curvature, makes bathymetry an essential infrastructure of the marine environment. Several methods include Single Beam Echo Sounding System (SBES), multibeam echo sounder, side scan sonar, airborne laser hydrography, multispectral satellite imagery, satellite altimetry, and most recently, in situ-unmanned/remote sensors can be used for bathymetry. However, available techniques have inherent uniqueness, and the choice for an application depends on many factors such as cost, product and benefits.

Acoustic multibeam and side scan sonars can provide increased sea bottom coverage, fine resolution and accuracy but require considerable time and cost to cover relatively small portions [11]. Airborne laser hydrography and aerial photography, which are faster techniques that enhance coverage to a large extent within a relatively short period of time, is practically very expensive, not ideal for water bodies with complex configuration due to maneuvering issues and not feasible for mapping turbid and deep waters as light only penetrates about 40m [11]. Unmanned/remote sensors such as tow fish and remotely operated vehicles require heavy financial investment in equipment and are not readily realizable in developing countries with meager economies [19]. Hence, many lakes, reservoirs, ponds, rivers and nearshore regions cannot be readily mapped [6].

Inadvertently, the non-availability of bathymetry in these economies greatly hinders maritime development, reduces water bodies' economic potential and thwarts navigational efforts. In situations of limited funds and where cost does not allow the use of other methods, depth can be precisely acquired with SBES to depict seabed morphology [35]. SBES provides accurate data that can be reliably and effectively used to map inland waterways [6, 15]. It is also useful for dredge operation, monitoring and evaluation [9, 34], production of bathymetric maps and nautical charts [18]. Besides, single-beam data are now used for seafloor habitat mapping [18] and as ground truth data for calibrating and validating satellite-derived bathymetry [13, 15].

Usually, SBES provides point-by-point sounding depths of the seabed and along the track of survey vessels. To create a depth surface that depicts the variable and continuous seabed morphology, interpolation is required to estimate the depth value for non-sampled locations [3, 12]. The lack of consensus on the best interpolation method for bathymetric data raises the need for evaluating methods that will provide the best results for specific sites and datasets [4]. This study assesses the capabilities of single beam sounding data in determining bathymetry characterization of the Imo River. Objectives of the study included comparing the accuracy of five interpolation methods in producing continuous bathymetry from SBES data, production of bathymetric profiles, depth derivatives and 3D bathymetry metrics.



2. Background

River bed topography is a variable and continuous surface, but depths measured with SBES are usually obtained as sets of spatial discrete point values. Essentially, data depicting continuous surfaces or phenomena are usually subjected to spatial processing to derive continuous surfaces for a unique representation of the phenomena [12,14]. Since it is impossible to take measurements at every location in an area of interest, spatial interpolation estimates values of unknown locations based on sets of functions from values of measured locations within the field. It is used to build continuous datasets from discretely measured sparse points. The interpolation process yields continuous data in a gridded format, usually as a digital elevation model grid [4,2]. Interpolation works on two principles of defining neighborhood area and neighboring values for determining unsampled point value [28]. Each technique has its peculiarities, assumptions and algorithms, such that the accuracy of each process depends on data sample size, the spatial distribution of sounding (sampling) points and resolution, seabed characteristics, boundary demarcation, and data set normality [21,16]. Reference [3] noted that different interpolation methods yield varying elevation surfaces even for the same project site and dataset based on underlying mathematical models. Thus, the choice of interpolation technique should be site-specific, have data characteristics and be based on the research application.

Interpolation can be distinguished as global, local, exact and inexact based on the behaviour of mathematical algorithms used in deriving values for unknown locations [3]. The global interpolation technique uses all measurements for prediction, while local techniques use specific data surrounding unknown locations to make predictions. The exact interpolators usually make predictions comparative to values of surrounding points, whereas inexact techniques make predictions without consideration of local peculiarities and constraints [3]. Usually, local methods use a specified number of points within a specified radius of the unsampled point's location to determine the value of each unsampled point's location [26].

Interpolation methods are broadly categorized in several pieces of literature into deterministic and geostatistical [28,38,21, 16]. The geostatistical method operates by fitting a spatial model to sampled data to generate prediction values at unsampled locations. Usually, geostatistical interpolation estimates the prediction accuracy, unlike the deterministic technique [3,4,38]. Geostatistical interpolation methods have the advantage of calculating errors associated with the measurement, creating a prediction error map, and using mathematical and statistical functions to predict point values [31,3,38,16]. A statistical function or stochastic model is an autocorrelation function that defines the statistical relationships between predicted points and the different

measurement points within a data set. This spatial correlation controls the distance and direction of points used for prediction. Together with a defined number of points and set radius, it helps to determine unsampled point values with high accuracy [38,2]). The basic tool of geostatistics is the semivariogram. Semivariogram captures the spatial dependence between sample points by plotting semivariance against separation distance. Example of geostatistical interpolation includes ordinary kriging, universal kriging, simple kriging, Empirical Bayesian Kriging, regression kriging and areal interpolation.

Deterministic interpolation methods use priori models or mathematical functions to predict values at unsampled locations without considering spatial data distribution. Unlike the geostatistical method, deterministic techniques weigh measurement values of sample points directly and apply the same in predicting values for unknown locations. It lacks provision for uncertainty assessment of predicted values such that predictions which are accurate or flawed cannot be spotted in the interpolation output [4, 3, 38, 16]. Deterministic techniques include inverse distance weighted, radial basis functions, triangular irregular networks, and global polynomial and local polynomial interpolation [3,38]. A few interpolation methods considered and adopted for this study are discussed briefly.

Ordinary Kriging (OK) is a fundamental geostatistical interpolation technique that uses a linear-weighted approach to predict values from a stationary random field for unknown points in an unbiased estimation [38,16]. OK assumes intrinsic stationarity of data with the condition that the mean of measurements used to predict point value is unknown but constant. It relies on ample observations to estimate the variogram, an average of a subset of neighboring points calculated based on the assumption of normality among data points. With random spatial stationarity sampling, OK produces unbiased estimates with minimized error variance [38,16].

Reference [38] expressed the fundamental formula for OK as:

$$Z(x) = \sum_{i=1}^n W_i Z_i \tag{1}$$

Where, $W = \frac{1}{d_i^k}$ (2)

Then, $Z(x) = \sum_{i=1}^n \frac{Z_i}{d_i^k}$ (3)

To eliminate bias, it is assumed that the sum of interpolation weight must be unity (equation 4)

$$\sum_{i=1}^n W_i = 1 \tag{4}$$

As a geostatistical interpolation method with random spatial stationarity sampling, OK considers spatial data distribution and produces unbiased estimates with minimized error variance. The error variance (σ^2) defines the measure of

uncertainty in the prediction and, according to [38], is expressed as:

$$\sigma^2 = \frac{\sum_{i=1}^n (Z(x) - Z_i)^2}{n} \quad (5)$$

From the equation 1-5;

Z = estimated value at a predicted point,

Z_i = observed value at point i.

W_i = weight value assigned at point i,

d_i = distance between the point I and the predicted point;

k = power variable.

n = total number of data points used in the interpolation process.

Inverse Distance Weighting (IDW) is a deterministic interpolation method that uses measured point values to predict the value of unmeasured locations based on the distances from the known points. IDW works by assigning weight to the inverse of distances of neighbouring measured points and on the assumption that closer points are more related such that weights decrease rapidly as distance increases [26]. IDW, according to [14], assumes that ‘each measured point exerts a local influence, which decreases with distance’ such that distant points are assigned lower power [38]. IDW interpolation function, according to [26], is expressed by equation 6:

$$Z_{x,y} = \frac{\sum_{k=1}^N \frac{z_k}{d_k^p}}{\frac{1}{d_k^p}} \quad (6)$$

Where;

Z_{x,y} = estimated value at the position (x,y) of the grid,

z_k = a neighbouring data point value,

N = the number of neighbouring points,

d_k = the distance between the data point and the point being interpolated,

p = a positive-power parameter, also known as power variable.

Like OK, IDW produces an optimum result where evenly spaced and large measurement data are used [14]. However, IDW does not take cognizance of spatial data distribution, but predictions are the linearly-weighted average of sample points [3,16]. Instead, IDW, as an exact interpolator, predicts point values identical to input measured points. IDW is computationally simple but has the disadvantage of using ‘neighbourhoods’ data within a circular range with similar weight averages to estimate values [12,14,16]. It also causes much smoothing in resulted interpolated surface, leaving ‘flattening peaks and valleys’ [28].

Radial basis functions (RBFs) is an artificial neural network tool that contains diverse functions, each with parameters that fit a smooth surface through measured points. These parameters have different shapes and minimize overall surface curvature such that each RBF interpolation result is slightly different from the other [14, 4,26,38].

Whatever the function, RBFs are exact interpolators that fit a smooth surface through measured point values to generate interpolated surface (value) based on the relative distance of interpolated points to a specified sample point. In the process, each basis function ‘determines which plane (surface) matches in-between the values’ [14]. RBF interpolation usually produces superior output in regions of fair undulations but with a poor result where the bathymetry has complex nature with large changes in depth. Substantial data uncertainty affects RBF poorly but is very flexible in producing interpolation surfaces [14,2]. Interpolation functions of RBF include completely regularized spline, spline with tension, thin-plate spline, multiquadric function and inverse multiquadric function [14,4,26]. Multiquadric function and inverse multiquadric function were used in this study. The general principle of RBF can be expressed by equation 7.

$$\hat{Z}(s) = \sum_{i=1}^N \omega_i \varphi(\|s_i - s_0\|) + \omega_{n+1} \quad (7)$$

Where φ is the basic radial function expressed as $\varphi(r)$, then for thin-plate spline and multiquadric, the functions are expressed by equations 8 and 9, respectively.

$$\varphi(r) = (\sigma + r)^2 \ln(\sigma + r) \quad (8)$$

$$\varphi(r) = (r^2 + \sigma^2)^{1/2} \quad (9)$$

From the equations, $r = \|s_i - s_0\|$ is the radial distance between the point for which a new value (s_0) is calculated and the points with measured values (s_i); Ψ is the weight value assigned at the point interpolated point [4].

2.1. Review of Literature

A review of related and relevant works of the literature revealed performances of different interpolation techniques across different study areas based on datasets. In a study to construct 3D bathymetric models for the Gulf of Pozzuoli, Italy, [26] reported thin-plate spline - radial basis function (TPS-RBF) algorithm, OK and UK techniques as having better performances (among fifteen interpolation methods). Comparative performance of seven interpolation methods (OK, OKA, UK, IDW, EIDW, RBF and LPI) for mapping of Lowermost Mississippi River tested the consistency of the interpolation methods over the entire river channel. It concluded that the thin-plate spline-radial basis function (TPS- RBF) algorithm had the overall best performance [35]. The study summary reported OK as the most widely used interpolator method in studies of river channel bathymetry within the USA and other places [35]. IDW was used as a baseline interpolant in a comparative case study to ascertain the acclaimed sophisticated performance of EBK and random forests machine learning methods [37].

Performance and accuracy evaluation for bathymetry map construction of Saldanha Bay, graphic illustration and statistical analyses were executed by [18]. The study adjudged IDW and OK techniques as the best-known and commonly used interpolation methods. Results of the study indicated that both IDW and OK interpolations produced a similar effect and generated continuous bathymetry output, although IDW had finer statistical performance in all interpolation tests. Reference [18] presented IDW as the most preferred method for interpolating bathymetry for Saldanha Bay, South Africa. [18] documented several studies that adopted IDW and kriging interpolation techniques to derive accurate seabed bathymetry. Work by [36] revealed universal and OK interpolation techniques for comparative prediction statistics and map output with fine root mean square error.

3. Materials and Methods

As part of the bathymetry investigation of the lower section of the Imo River for the purpose of safe navigation, a single-beam bathymetry survey was conducted. The data processes covered tidal observation and sounding; interpolation analysis; production of digital depth model (DDM), bathymetric profile, contour, slope, aspect, bathymetry position index and bathymetry. The riverbed geomorphological analyses were also performed based on slope, aspect, and bathymetric position index. 3-D Analyst, Spatial Analyst and Geostatistical tools of ESRI ArcGIS 10.5 and Benthic Terrain Modeler toolbox, Surfer 23 and Excel Microsoft Spreadsheet were adopted for the processing. The work process adopted is presented in the flow diagram (Figure 1) and discussed in the subsections below.

3.1. Study Area

The study covers a 2.7 km lower section of Imo River (Figure 2) lying within the geographical boundaries of latitudes 4° 28'N and 5° 00'N and longitudes 7° 10'E and 7° 40'E. The section is located in the southern tip of Nigeria in the Niger Delta region (Figure 2). Imo River has a mesotidal pattern with a tidal range of 2.20m to 2.50m [35]. Depth ranges within the study area are between -0.66 and 12.96m above the datum. It lies within a relatively flat topography usually influenced by the tidal regimes of the Atlantic Ocean.

3.2. Data

South SDE-28 Single Beam Echo Sounder integrated with Hi-Target DGPS GNSS Receiver was used to conduct a bathymetry survey in January 2021. A total of 1968 points were acquired. Direct tide observation based on a manual tide gauge was carried out for vertical referencing during the sounding period. It was later analyzed to determine the proper tidal datum to which the sounded depths were reduced. Analysis of tide and predictions yielded Z0, MSL tidal components and type of tide [35]. To account for tidal fluctuations and enhance the consistency of acquired depths regarding datum, sounded depths were vertically referenced

and reduced to mean water level (MWL) datum by applying equation 10 in Microsoft Excel 2007 software.

$$Reduced\ depths = MWL - Sounded\ depths \quad (10)$$

MWL was the adopted datum with a value of 1.660 m and sounded depths were in-situ depths measured with the echo sounder.

The bathymetry survey carried out was according to the International Hydrographic Organization special order since under-keel clearance was critical for safe navigation. For special order survey at a 95% confidence level, depth accuracy (bathymetric uncertainty) expressed by total vertical uncertainty (TVU max) according to IHO S-44 specification (IHO, 2020) is defined as:

$$TVU_{max}(D) = \sqrt{a^2 + (bXd)^2} \quad (11)$$

To calculate the error limits for depth accuracy, given that $a = 0.25$, $b = 0.0075$ and $d = 12.960$ m, the TVU max (D) was 0.268. The result indicated that the depth data meets the IHO special order standards. Thus, the x,y, and z SBES data was horizontally and vertically referenced and saved in MS Excel formats. Figure 3 is a histogram showing the spatial range of acquired data.

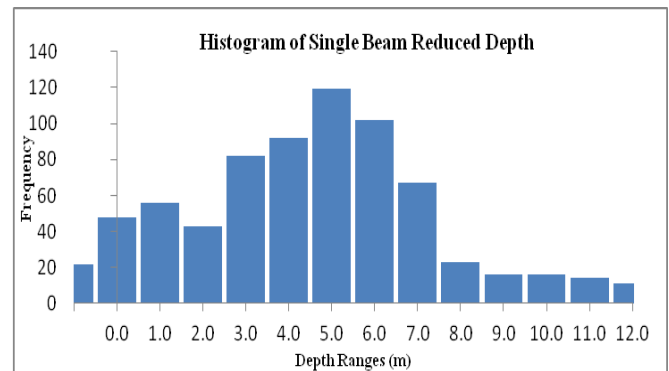


Fig. 3 Depth distribution of single beam data

3.3. Interpolation and Production of Digital Depth Model

Interpolation of the irregularly spaced sounding data was carried out to create a regularly spaced grid surface before the two-dimensional or three-dimensional model of the riverbed was achieved [12,14,2]). To determine the best interpolation method for the dataset and study area, as well as the accuracy and quality of generated digital model, two deterministic and two geostatistical interpolation methods, were used. These included inverse distance weighting, radial basis function (multi-quadric and inverse quadric), ordinary kriging and universal kriging. The choice of interpolation methods was based on the wide application for bathymetric data processing [14, 4, 16]. The assertion by [6] that surfer is ‘a more specialized gridding and 3D surface mapping program than ArcGIS’ was tested by statistically and visually

comparing the interpolation depth grid result from the two software. Surfer 23 and ArcGIS 10.5 software versions were used for this purpose.

The reduced XYZ SBES data file of the project site was imported into a surfer and interpolated to produce a 3D surface (digital depth model). Likewise, the SBES data file was also imported into ArcGIS as a ‘point file’ and ‘event layer’ were created. The event layer generated an array of pixels (grids) - bathymetric 3D surface (digital depth model). The digital depth model (DDM) is a marine equivalent of the topographic digital elevation model (DEM). In the marine context, DDM is a 3-Dimensional representation of the river bed relief as an array of pixels. The resultant digital models from the interpolation processes and the two software were compared to determine the best fit for the study.

To determine the best interpolation method, interpolation results can be evaluated based on the comparison of semivariogram, visualization of generated DDM, cross-validation [21] or analysis of statistic parameters ([4], [26]). But usually, the overall best performance of an interpolation method was based on the closeness of interpolated values to reference data [26]. Also, analyses of statistic parameters - minimum, maximum and mean of the in-situ and interpolated points, as well as the standard deviations (Std. Dev.) were applied. Statistics of the DEM obtained from the five interpolation methods were compared with the statistics of the SBES data. These are presented in Table 1, with 3D visualization of the resultant digital models presented in figure 4.

As indicated in Table 1, statistics from the interpolation methods from ArcGIS had sizeable differences from the SBES data, whereas results from surfer had less variance. RBS_INVQD had the least minimum and maximum and meant depth value difference of 0.247m, 0.021m, and -0.321m, followed by IDW, with a difference of -0.617m. For UN_KRG, the differences in depth ranges were quite obvious, while RBS_INVQD had the lowest depth difference but the highest standard deviation. OK had differences similar to that of the RBS_INVQD result.

From figure 4, it was inferred that OK interpolation produced a more accurate DDM followed by RBS_INVQD output, which gave a 3D surface very similar to that of ordinary kriging but with minor discrepancy. The IDW DDM has a much smoother representation, with fewer artifacts than UN_KRG and RBS_MQD. Generally, interpolation results from Surfer (Figure 4b) yielded better grid surface than ArcGIS (Figure 4a).

Table 1. Statistical result for interpolation methods

Method/ Statistics	Min.	Max	Mean	Std. Dev.
SBES data	-0.660	12.960	4.675	2.594
ArcGIS				
OK	-0.423	12.185	4.320	1.783
UN_KRG	-24.516	44.244	4.037	2.520
IDW	-0.610	12.673	4.306	1.799
RBS_INVQD	-1.634	13.001	4.346	1.179
RBS_MQD	-1.225	12.992	4.285	1.822
Surfer				
OK	-1.277	12.847	4.279	1.833
UN_KRG	-2.589	12.847	4.147	1.967
IDW	-0.349	12.751	4.324	1.741
RBS_INVQD	-0.413	12.981	4.354	1.733
RBS_MQD	-2.590	12.990	4.184	1.910

OK = Ordinary Kriging, UN_KRG = Universal Kriging, IDW = Inverse Distance Weighting, RBS_INVQD = Radial Basis Function Inverse Quadric, RBS_MQD = Radial Basis Function Multi-quadric.

Based on the indicators (Figure 4 and Table 1), OK and RBS_INVQD methods tend to have better performance than IDW and RBS_MQD, while UN_KRG gave the worst outcomes. From the analysis result, the OK method was used for generating the riverbed 3D surface for the study area. The gridded 3D surface from surfer was exported in a compatible extension format (.tif) into ArcGIS for further processing and rendering.

3.4. Production of 3D Derivatives

Digital bathymetric models can be used for morphometric analysis, such as seafloor classification, object detection and in deriving terrain descriptors [36]. Besides, bathymetric data could be presented in several formats and styles, depending on its intended purpose. Major classes of terrain parameters obtainable from bathymetry data include slope, aspect curvature and rugosity [37]. Slope and aspect are first-order derivatives of bathymetry as they are derived directly from the DDM. In contrast, local mean, curvature and rugosity are second-order derivatives obtainable from the slope. Accordingly, further analysis and derivation of geomorphometric measurements of the riverbed were executed. These terrain parameters, including the bathymetry position index, were calculated using the ‘Benthic Terrain Modeler’ toolbox in ArcGIS 10.5.

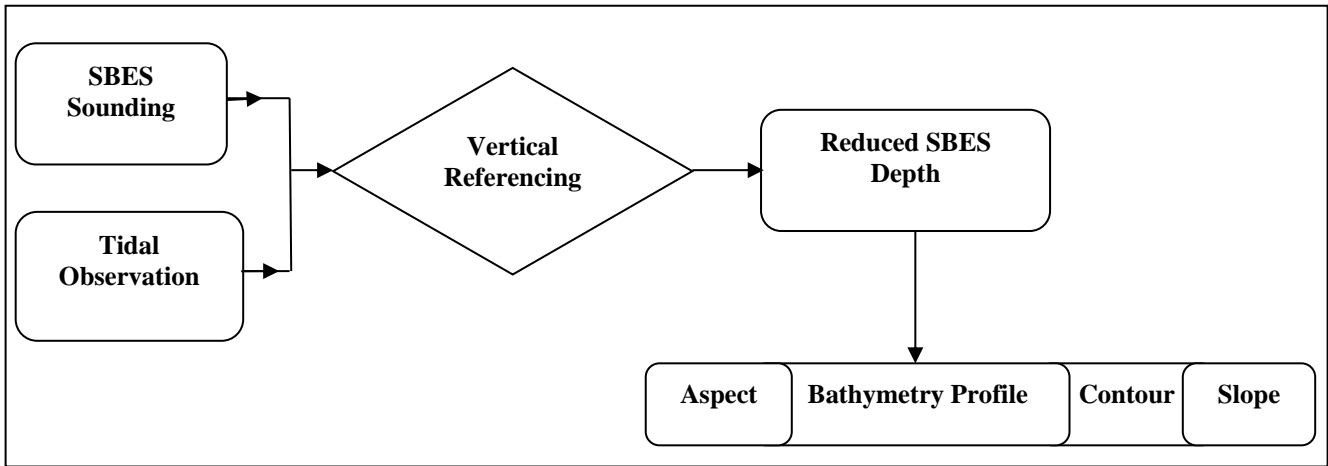


Fig. 1 Methodology flow diagram

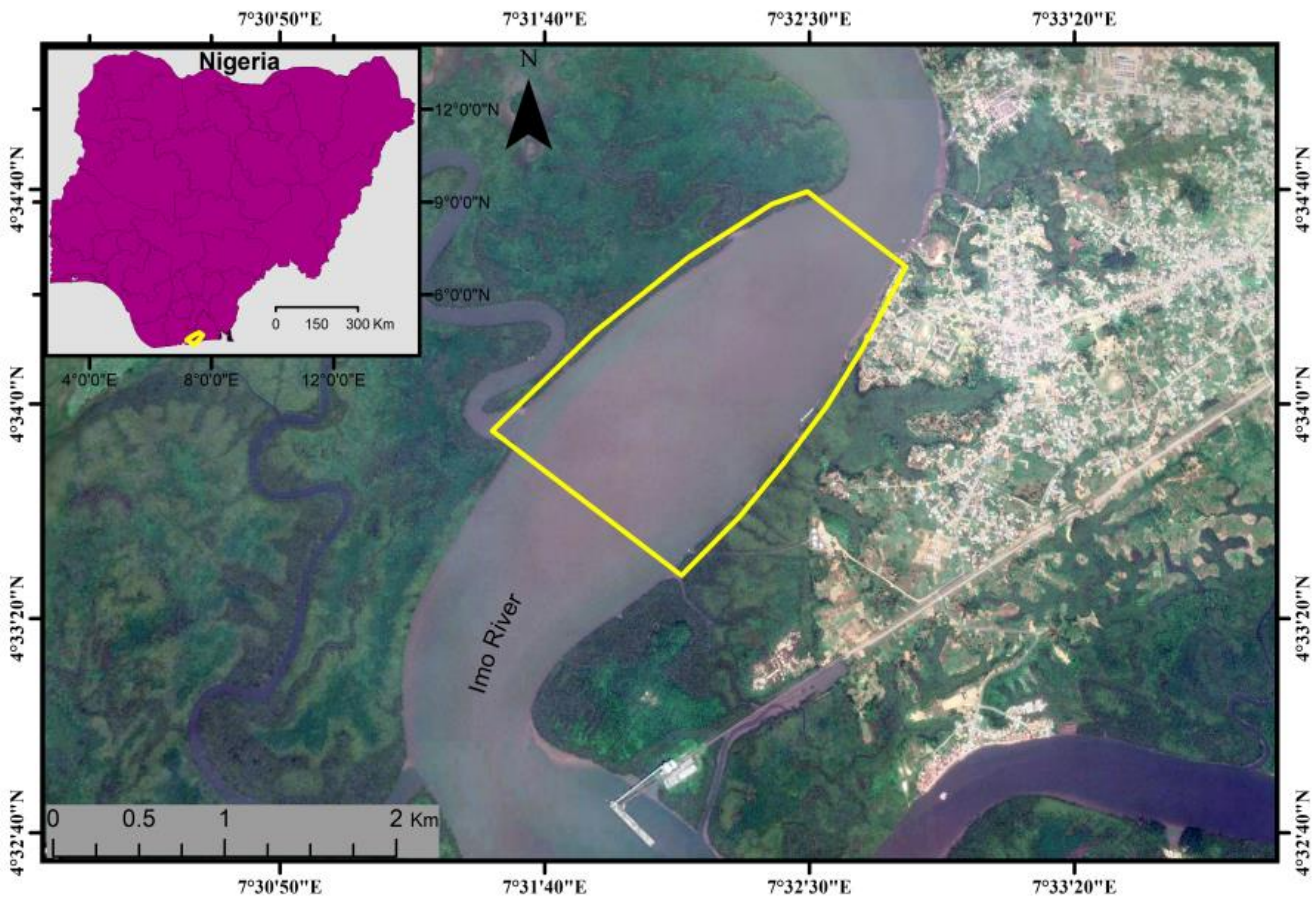


Fig. 2 Map of the study area

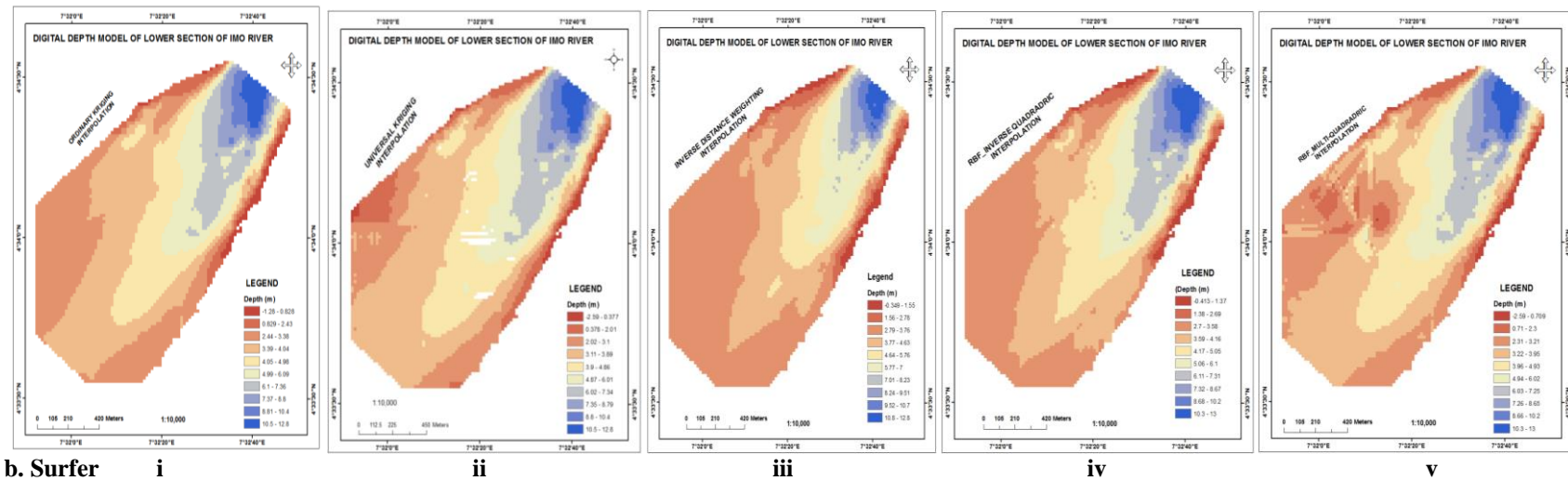
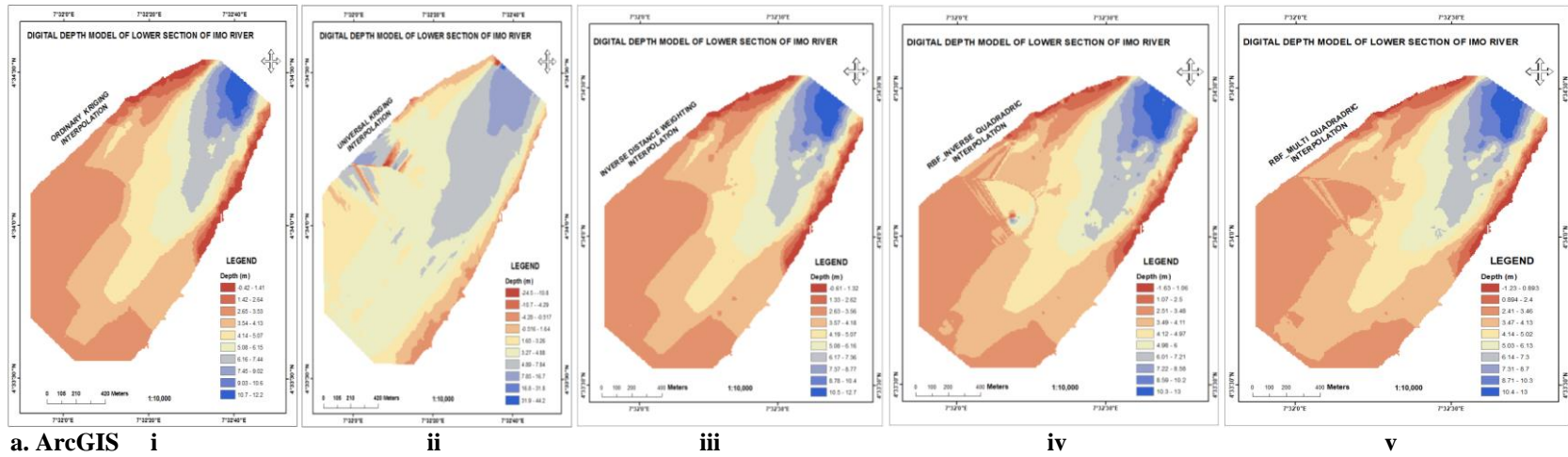


Fig. 4 3D-Surface (digital depth model) from (A) Surfer 23 (B) ArcGIS 10.5 software (i-Ok, ii- UN_KRG, iii- IDW, iv- RBS_INVQD, v- RBS_MQD)

4. Results and Discussion

4.1. Interpolation Output

Based on the analyses (section 3.3), ordinary kriging interpolation from Surfer 23 software yielded the best interpolation surface due to the fact that the DDM generated was consistent with the slopes and curvatures of the river bed [23]. The 3-D (bathymetric) grid was used to generate bathymetric contour, shaded relief, longitudinal depth profile and 3-D derivatives for the river. Figure 5 is the digital depth model (DDM), while the contour map and shaded relief of the study area are presented in figure 6 and figure 7, respectively.

The DDM (Figure 5) shows the river bed relief over ten ranges with different colours. The river's deepest section (deep blue) ranges between 10.5m to 12.8m below the datum, while most shallow areas (red-brown/burnt umber) were between -1.28m above the datum and 0.828m below the datum. The model also revealed that major parts of the river were shallow. Figure 6 shows the relief of the Imo

River by contour lines. Each contour line defines the depth of points on the riverbed with respect to the mean water level. The northwest and northeast sections reveal a region of steeper bathymetry gradient, while the southwest indicated fairly flat bathymetry. The contour map (Figure 6) vectorally depicts and corresponds to the raster representation of the river bathymetry given by the slope map (Figure 10).

Figure 7 is a hill shade map portraying the sun's effects of illumination based on depth variations in the situation of direct sunshine on the river bed. It provides a gray-scale visualization of illumination on the river bathymetry and aids in interpreting seafloor topography through the shading and shadows on crests and depressions [29]. Since illumination of positions on the river bed is a factor of slope and aspect, figure 7 qualitatively displays a high lighting effect on the Northwest aspect slope (see Figure.10). In contrast, a region with a steep slope (Figure 9) and east aspect (Figure 10) had low intensity. A fairly undulating slope area with a westerly aspect displayed medium-intensity illumination.

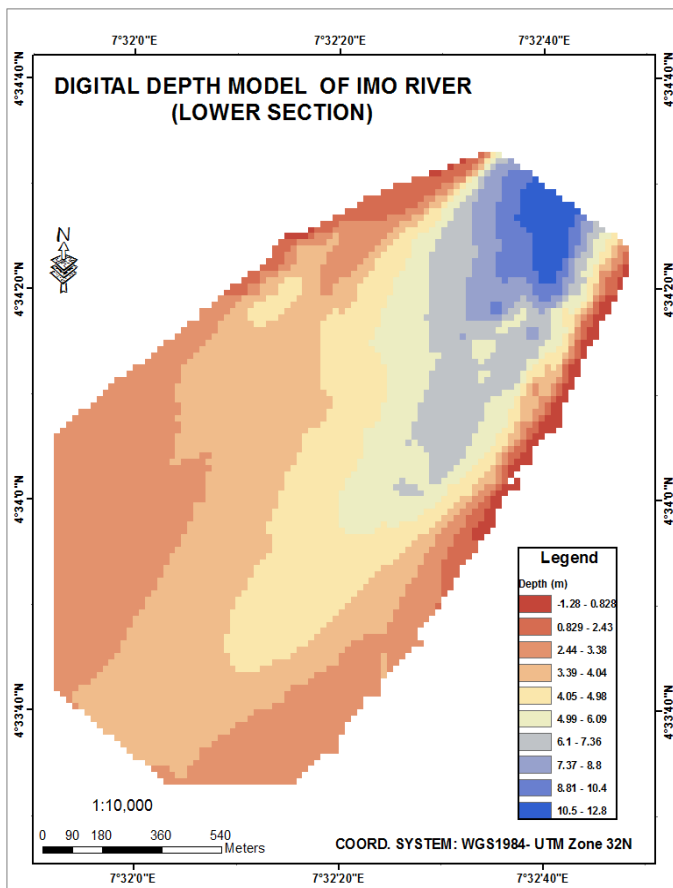


Fig. 5 Digital (Bathymetric) Depth Model

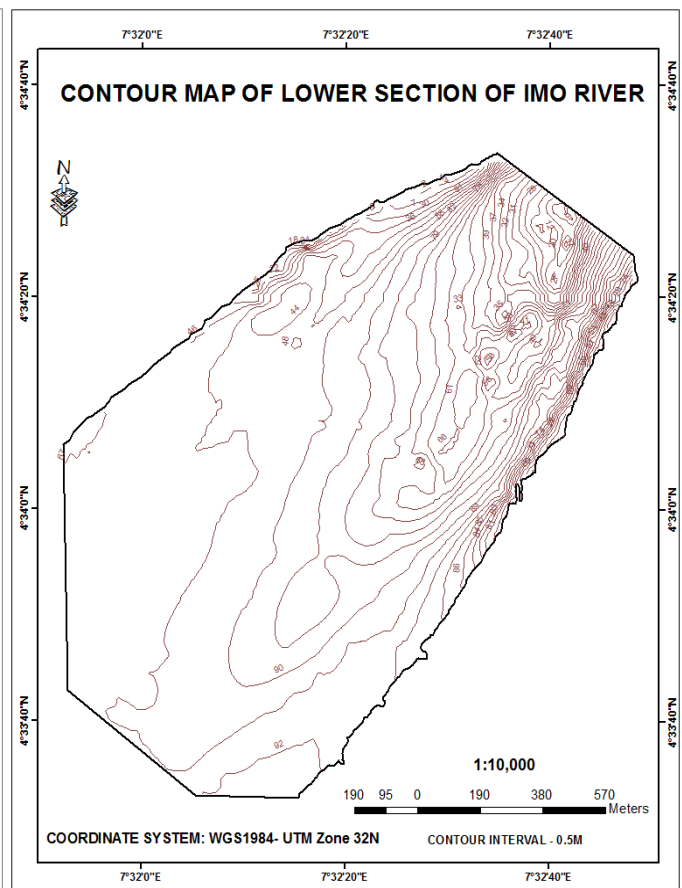


Fig. 6 Contour map

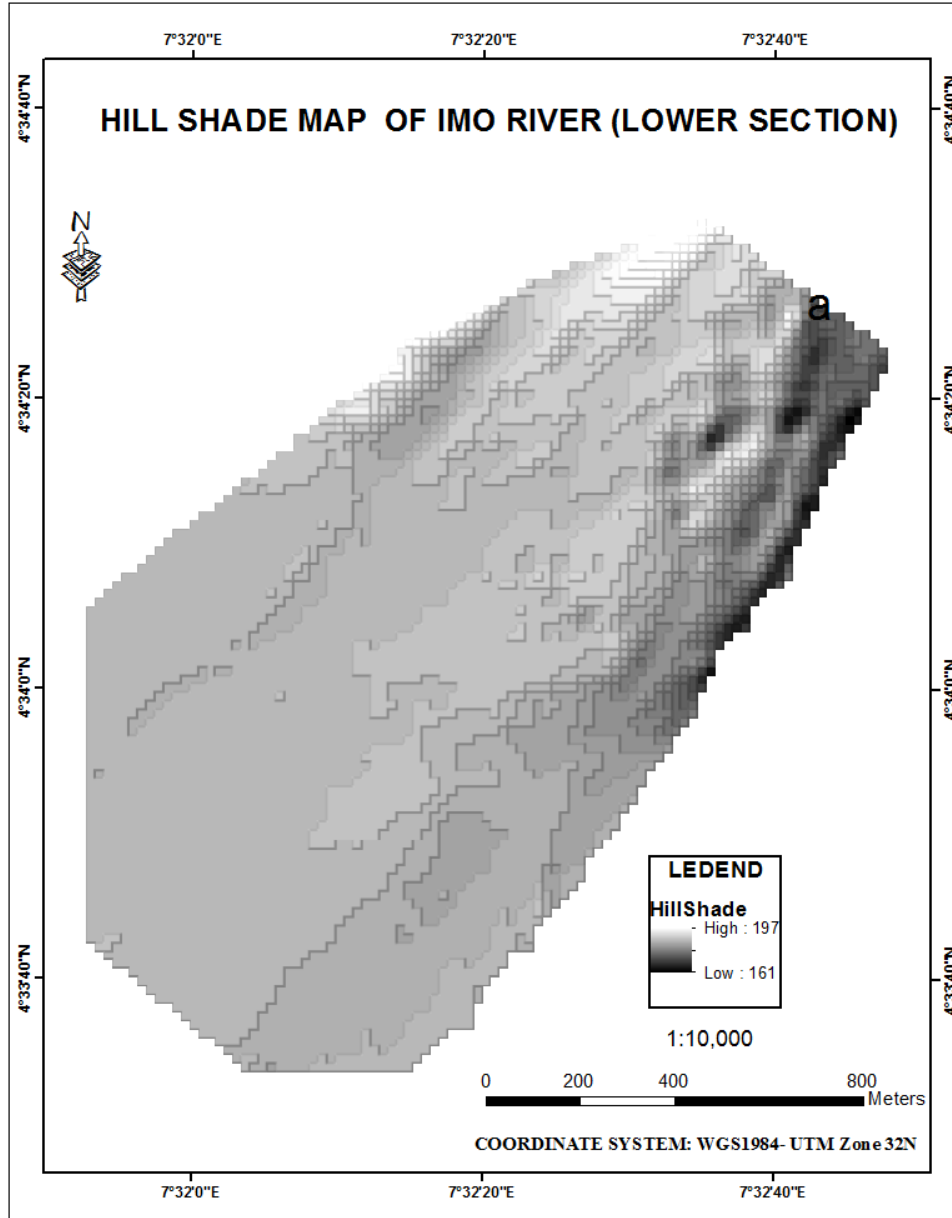


Fig. 7 Hill shade map

4.2. Bathymetric Profile

Bathymetric profiling was done to obtain a longitudinal profile view of the riverbed. A bathymetric profile is a plot of river depth against upstream to downstream distance ‘where hills are seen as rises and valleys as depressions’ [8]. It allows for a closer examination of bathymetric variations along the river channel. The bathymetric profile (Figure 8) was generated from a line feature drawn over the DDM along the left (west), centre line (middle) and right (east) sections of the river channel. The bathymetric profile with a north-south orientation show changes in depths along the river's course. It reveals that the river is deeper at the inland area around the ‘Boat Yard’ and shallower as it traverses towards

the ALSCON jetty area, some kilometers from the Gulf of Guinea. The deepest point was 12.9m below the datum, located close to the boatyard just after the meandering point along the course of the river. The shallowest depth was - 0.66m above the datum. It also indicated that sediments tend to move from the inland part of the study area towards the ocean. This indicates sediment and other materials tend to be swept downstream along the river due to wave and tide action. However, the depositional action making the water shallower was due to fishing activities as several wooden poles used as a barricade to hold fishing nets placed by fishermen were found dotting the shallow portion of the river.

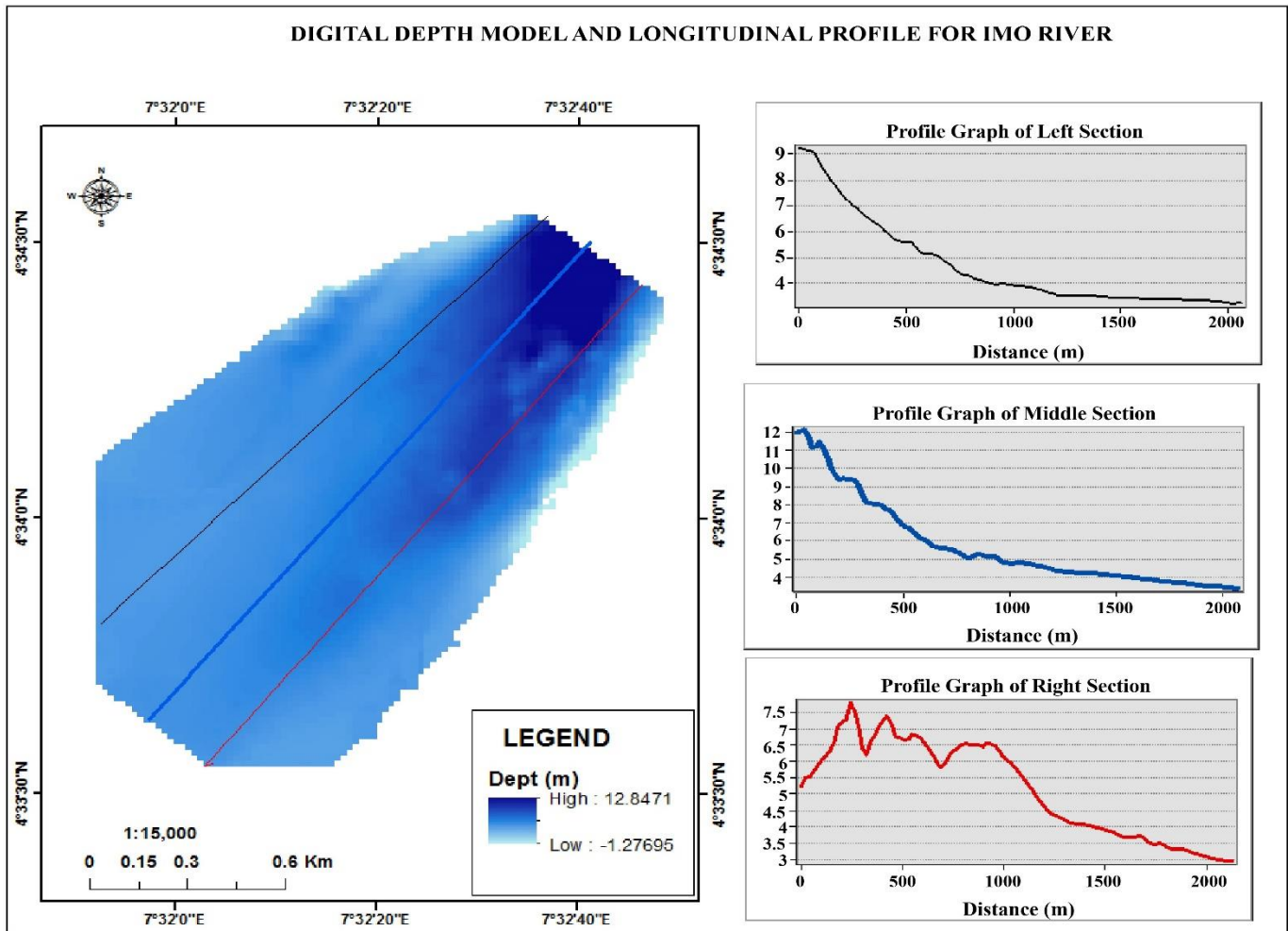


Fig. 8 Bathymetric (Longitudinal) profiles for the Lower Section of Imo River

4.3. Calculation of Slope

The slope may be defined as the measure of steepness or the maximum rate of depth change [7]. It is a bathymetric gradient that shows the maximum rate of change of depths in a river [3]. Slope output values for a 3 x 3 screening window of raster grids are the maximum rate of change from the focal pixel to its surrounding pixels. Values of slope generated as 0 (lowest) depict a flat area indicating that the pixels around the focal pixel are equivalent to the depth value of the focal pixel [32]. A lower slope value indicates gentle undulating terrain, while a higher slope value indicates steep terrain. However, the maximum slope value depends on the seabed characteristics and raster resolution and output. Slope raster can be calculated in two types of units, degrees or percent (percent rise) [32]. Thus, the slope raster presented in figure 9 revealed the gradient of the study area in radians.

The slope statistics (Fig. 9) had values ranging between 0.0017212% (Low) to 5.84893% (High). Based on slope percentage, the river section can be classified as a steep stream as the slope is above 4% [16]. The slope gradient at

the northeast and North West region is high (blue shading) but gradually reduces as the river traverses south towards the crestal area (green). Areas with low slope values tend to support shallow water communities in the study area, as fishing activities were noticed within this region.

4.4. Calculation of Aspect

Aspect measures surface direction and reflect the orientation of a given point or location on the river bed. In a raster bathymetric grid, the aspect gives the compass direction of each cell's gradient. It defines the easternness and northerness of underwater relief [36,37,7]. Usually measured in the unit of degrees (°) and a clockwise direction from 0° (north) to 360° (north), the value of each cell in an aspect dataset indicates the direction the cell's slope faced. 0° is true north, a 90° aspect points to the east, 180° is south-facing while 270° directs to the west. Based on computation results, flat regions with no slope orientation are assigned a value of -1 [36]. Bathymetry influences both local and regional currents and directly impacts marine and coastal hydrodynamics [37].

With the Benthic terrain module (BTM), the aspect can be transformed into two linear scales; cosine and sine, to check modeling violation in contexts of circular model [36]. While the cosine scale gives the Northernness (A_N) function representing north–the south direction, the sine scale or Easternness (A_E) aspect represents the west–east slope [36]. Mathematically, these scales are represented as:

$$A_N = \cos(A): -1 \leq A_N \leq 1 \quad (12)$$

$$A_E = \sin(A): -1 \leq A_E \leq 1 \quad (13)$$

Figure 10 shows the output aspect raster for the data set. Fig. 11 a is the cosine aspect scale with values ranging from -1 (south) to +1 (north), while Figure 11b is the sine scale with -1 (west) to +1 (east) aspect. From the map (Figure 10), the riverbed tends to slope in the southeast direction around the Marine Police Jetty (Ikot Abasi). This explains the phenomena often experienced during high and low tides when mangroves and other debris are usually transported towards the Marine Police Base. Visual inspection and history of the area revealed that most flooding was usually experienced at the bulwark, with much dirt transported by the river. North-facing slopes are comparatively very small compared to another cardinal tilting seascape in the study area. Thus, sediment is usually carried down the river.

Figure 11a (northernness aspect scale) revealed that the north-south oriented slopes are more pronounced in the western section of the map, having positive values indicating the north-facing aspect and negative values for south-facing slopes. On the contrary, figure 11b (easterness aspect scale) revealed a low northernness slope (negative value) and high easternness aspect with positive value. This corroborates with the aspect output in figure 10.

4.4.1. Calculation of Bathymetry Rugosity

The undulating nature of the riverbed was assessed in the study by generating a rugosity map. Rugosity which may be referred to as the measure of surface roughness, terrain ruggedness or bumpiness, defines the roughness of the seafloor as the ratio of surface area to the planar area [25, 30, 36]. Mathematically, [36] defined rugosity as:

$$R = \frac{A_{\text{contoured area}}}{A_{\text{planar area}}} \quad (14)$$

Computation of rugosity with BTM can be executed using surface area to planar area, arc-chord ratio and vector ruggedness measure (VRM) [36]. VRM was chosen for this study because it uses local slopes and aspects to evaluate seabed heterogeneity or roughness [36]. With VRM, the orthogonal unit vector of a cell in a 3X3 moving window is decomposed using three-dimensional locations of the cell center, the local slope and the local aspect. After evaluation, a resultant vector for the window yields a dimensionless value ranging from 0 to 1 [25,36]. Zero value indicates no

variation, whereas 1 shows complete variation. Rugosity effectively captures the variability of slope and aspect in a single scheme [25] and can serve as an important parameter in ecological studies [30]

Figure 12 (rugosity map) is a raster surface that reveals the absolute surface elevation of the river bed for MWL [30]. The rugosity correlated strongly with slope (see Figure 9) such that regions of high rugosity corresponded to portions of high slope values, and lower rugosity related to a low slope. This goes a long way to establish the assertion by [29] that rugosity highly correlates with slope. This showed that the river bed is bumpier where there is much wave action, at regions where the river changes its direction close (point a) and at locations where a tributary joins the main river (point b). However, rugosity decreases as depositional action occur and becomes unnoticeable at places of high sediment deposit (point c).

4.5. Calculation of Bathymetric Position Index

Bathymetric Position Index (BPI) is a marine variant of the Topographic Position Index (TPI) useful for marine-based geomorphological studies and evaluation. BPI is a measure of the relative depth and slope of location on the seabed for the purpose of mapping seabed troughs and peaks, classifying coastal landforms based on the change in slope position. It defines the location of a specific bathymetric area in relation to other regions and features on the river bed. BTM computes BPI on two scales; Broad BPI and Fine BPI. Broad BPI is a scale with a wider spatial scope, while the fine-scale has a narrow scope whereby larger regions within the seascape can be identified. BPI is also set to identify and characterizing various benthic zones and structures by applying the Standardize FBPI and BBPI algorithm [30,1, 23, 29].

Computationally, the BPI tool calculates the mean elevation of cells and the difference between a focal pixel with others in a user-defined annulus. Where the surrounding cells are crests or ridges, BPI will have positive values and negative for positions near valleys. Areas with a constant slope will produce BPI values close to zero [30,36]. Figure 13a and 13b are the fine and broad-scale BPI generated from input bathymetry DDM. An annulus of 25 cells and 50 cells for inner and outer radius was used for fine-scale BPI computation, whereas 40 cells and 250 cells were adopted as inner and outer radius for broad-scale BPI. In Figure 13a, the FBPI calculates the bathymetry index into 6 classes (0-5), while BPI (Figure 13b) renders it in 7 class values from -1 to 6. The index value of 0 represents broad flat terrain in FBPI and BBPI, whereas 5 and 6 denote ridge in the FBPI and BBPI, respectively. Regions of lower BPI (1 and 2) revealed depressions and deeper depths. The low range of values for both FBPI and BBPI scales indicated less complex river bathymetry.

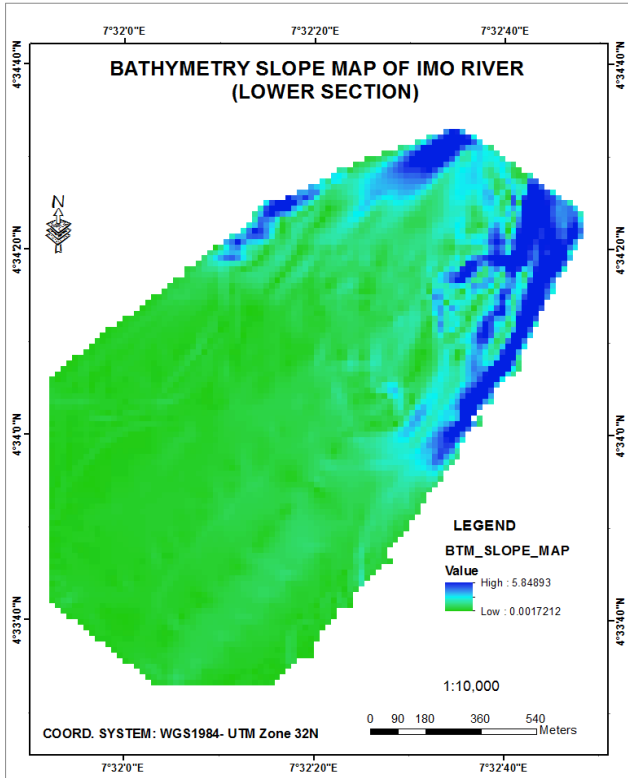


Fig. 9 Slope Map

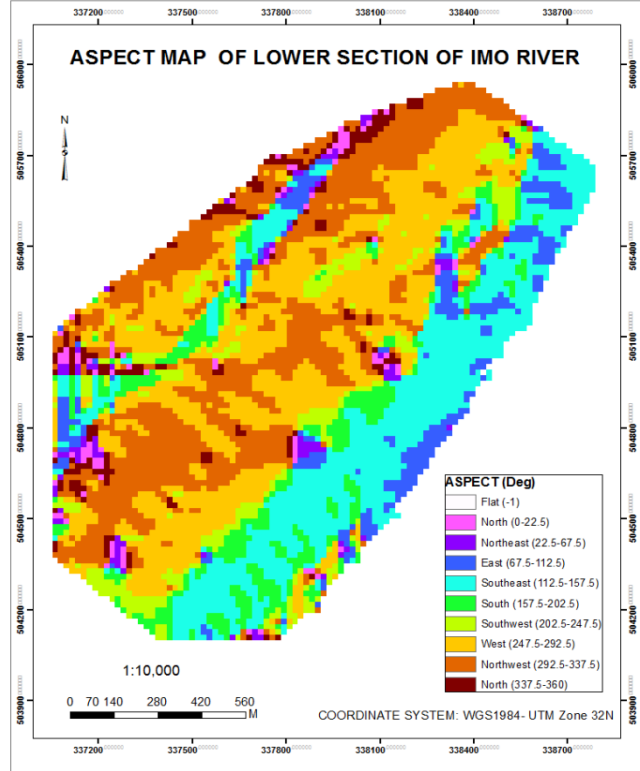
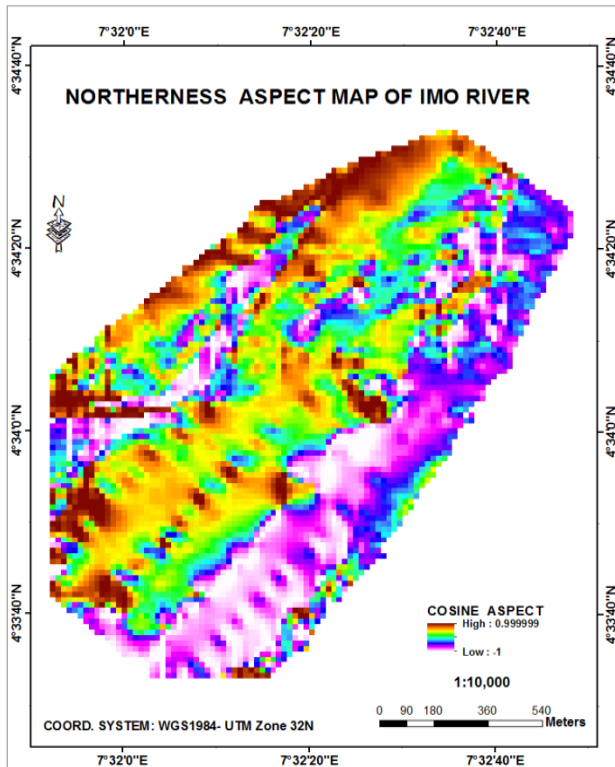
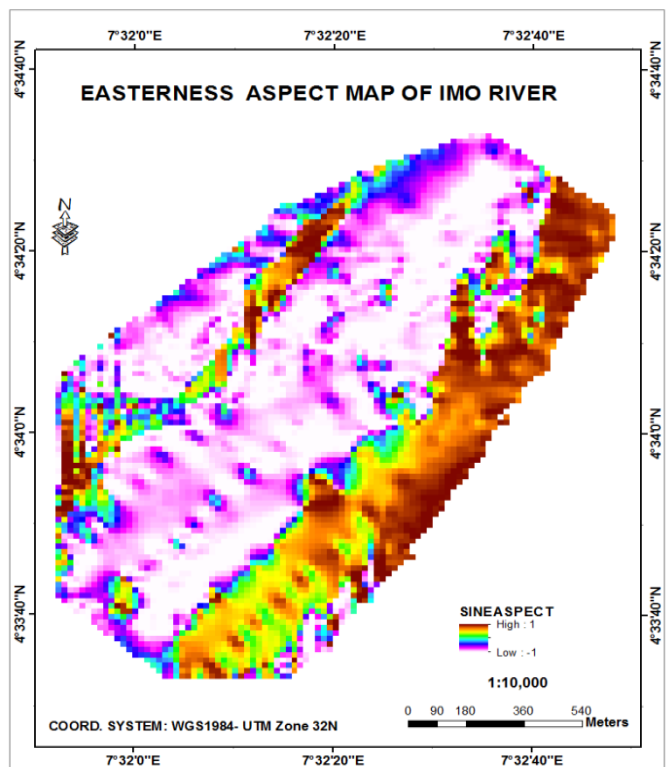


Fig. 10 Aspect map of the study area



(a)



(b)

Fig. 11 Cosine (a) and sine (b) aspect scale map

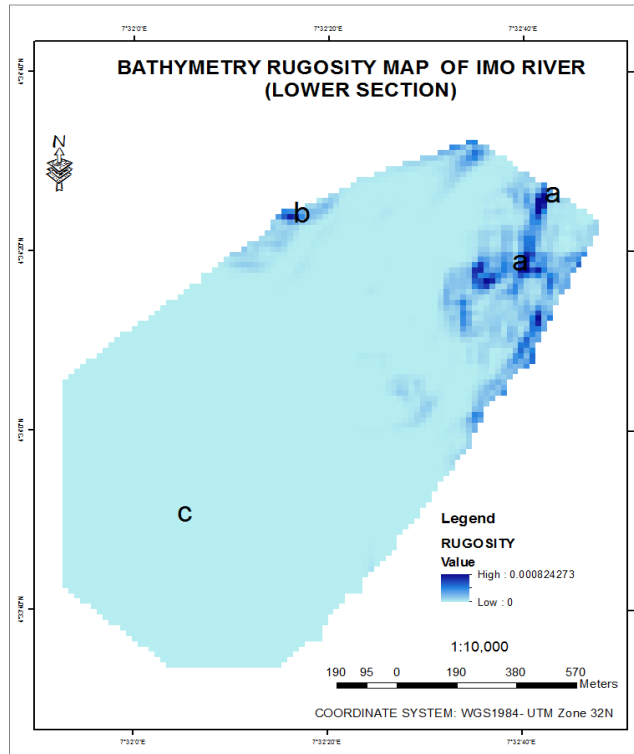
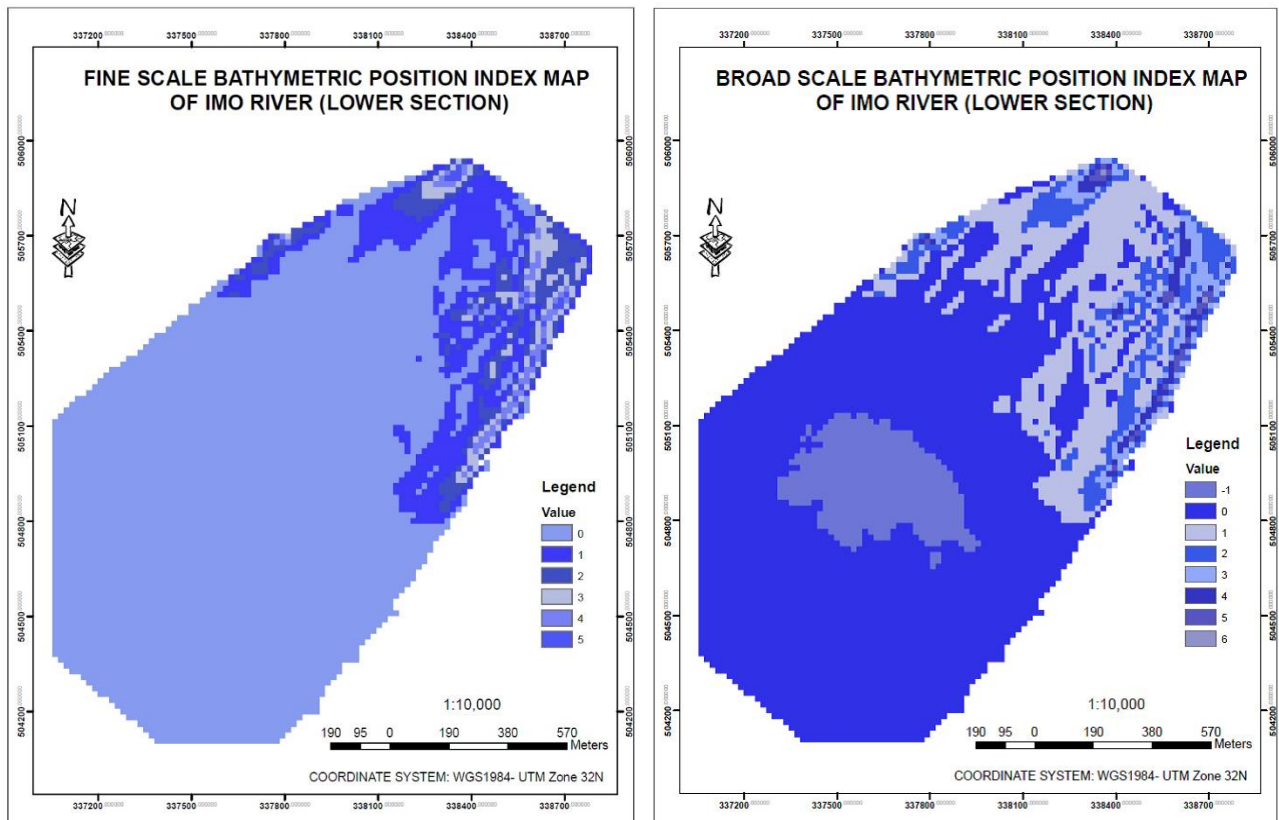


Fig. 12 Rugosity map



(a) (b)
Fig. 13 Bathymetric position index (A) fine-scale BPI (B) broad-scale BPI

5. Conclusion

This study mainly aimed to use single-beam echosounding data to generate 3D bathymetric models of the lower section of the Imo River. As an objective, the study assessed the interpolation method that provided the most accurate interpolation surface for the study area. Among the different interpolation methods tested, ordinary kriging executed in Surfer 23 software yielded the best representative of the river bed. This was because the DDM generated was consistent with the slopes and curvatures of the river bed. This highlighted the necessity for evaluating/assessing the effectiveness of interpolation methods in site-specific studies, data resolution and distribution. A continuous bathymetric grid of the river was produced, from which bathymetric profile, hill shade, slope, aspect, rugosity and

bathymetric position index were generated. The 3D models and profiles are versatile information for much regional research and operational purposes. These results proved effective in navigational safety analysis and will serve as data for calibrating and validating satellite-based estimated bathymetry. Although there were constraints during field operations, the study has demonstrated the unlimited use of single beam data in bathymetry mapping and analysis, which compares effectively with expensive bathymetry methods.

Acknowledgments

The authors acknowledge the contribution of Mr. Victor Effiong, who assisted in sounding data acquisition and staff members of the Divisional Marine Police, Ikot Abasi, who provided security during the sounding operation.

References

- [1] S. B. Agus, et al., "Mapping of Shallow Water Bathymetry and Reef Geomorphology Using Sentinel-2 Satellite Imagery in Genteng Besar and Genteng Kecil Island, Kepulauan Seribu," *Proceedings 4th International Conference Marine Sciences (ICMS 2021), IOP Conference Series: Earth and Environmental Science*, vol. 944, p. 012048, 2021. *Crossref*, <https://doi.org/10.1088/1755-1315/944/1/012048>
- [2] Sohaib Kareem Al-Mamoori et al., "Statistical Analysis of the Best GIS Interpolation Method for Bearing Capacity Estimation in an-Najaf City, Iraq," *Environmental Earth Sciences*, vol. 80, no. 683, 2021. *Crossref*, <https://doi.org/10.1007/s12665-021-09971-2>
- [3] Christopher J. Amante, and Barry W. Eakins "Accuracy of Interpolated Bathymetry in Digital Elevation Models," *Journal of Coastal Research*, vol. 76, no. sp1, pp. 123–133, 2016. *Crossref*, <https://doi.org/10.2112/SI76-011>
- [4] Maxim Arseni et al., "Testing Different Interpolation Methods Based on Single Beam Echo Sounder River Surveying. Case Study: Siret River," *ISPRS International Journal of Geoinformatics*, vol. 8, no. 507, pp. 1-21, 2019. *Crossref*, <https://doi.org/10.3390/ijgi8110507>
- [5] Spatial Data Interpolation: TIN, IDW, Kriging, Block Kriging, Co-Kriging: What Are the Differences? Aspxit's Website, 2019. [Online]. Available: <https://www.aspxit.com/spatial-data-interpolation-tin-idw-kriging-block-kriging-co-kriging-what-are-the-differences/>
- [6] A. B' Ardossy, Introduction to Geostatistics [Class Handout]. University of Stuttgart, 1997. [Online]. Available: <https://www.studocu.com/row/document/%d2%9baza%d2%9bstan-britan-tekhnikaly%d2%9b-universiteti/advanced-statistics/introduction-to-geostatistics-by-andras-bardossy/26548766>.
- [7] Bathylogger, Hydrographic Survey Single Beam Echo Sounder, 2018. [Online]. Available: <https://bathylogger.com/survey-info/>
- [8] Camila Brasil Louro da Silveira et al., "Coral Reef Mapping with Remote Sensing and Machine Learning: A Nurture and Nature Analysis in Marine Protected Areas," *Remote Sensing*, vol. 13, no. 15, p. 2907, 2021. *Crossref*, <https://doi.org/10.3390/rs13152907>
- [9] Docplayer.Net, Laboratory 2: Exercises 2 & 3 Bathymetric Profiles1 Based on the Chauffe & Jefferies, 2007. [Online]. Available: <http://docplayer.net/storage/65/52404326/52404326.pdf>
- [10] A. U. Ekpa, and N. I. Eyakndue, "Determination of a Section of Woji Riverbed Depths for Safe Navigation," *Nigerian Journal of Environmental Sciences and Technology*, vol. 1, no. 1, pp. 55 – 68, 2017. *Crossref*, <https://doi.org/10.36263/nijest.2017.01.0033>
- [11] Akwaowo Udo Ekpa, and Ito Ben Udo, "Tidal Trend Evaluation for Imo River Between 2013 and 2021," *SSRG International Journal of Geoinformatics and Geological Science*, vol. 9, no. 1, pp. 38-45, 2022. *Crossref*, <https://doi.org/10.14445/23939206/IJGGS-V9I1P105>
- [12] I. Elhassan, and Bathymetric Techniques, In Proceedings FIG Working Week 2015, Paper TS04A (7716), 2015. [Online]. Available: https://www.fig.net/resources/proceedings/fig_proceedings/fig2015/ppt/ts04a/ts04a_elhassan_7716_ppt.pdf.
- [13] Italo Oliveira Ferreira et al., "In Bathymetric Surfaces: IDW Or Kriging?," *Bulletin of Geodetic Sciences*, vol. 23, no.3, pp. 493 – 508, 2017.
- [14] Bassam Gabr, Mostafa Ahmed, and Yehia Marmoush, "Planetscope and Landsat 8 Imageries for Bathymetry Mapping," *Journal of Marine Science and Engineering*, vol. 8, no. 2, p.143, 2020. *Crossref*, <https://doi.org/10.3390/jmse8020143>
- [15] R. Gradka, and A. Kwinta, "A Short Review of Interpolation Methods Used for Terrain Modeling," *Geomatics, Land Management and Landscape*, vol. 4, pp. 29–47, 2018. *Crossref*, <http://doi.org/10.15576/GLL/2018.4.29>
- [16] Classifying Your Stream Slope, Greener Pasture Website. [Online]. Available: <https://streamhandbook.org/evaluating-your-property/classification/stream-slope/>

- [17] Nur Syahirah Hashim et al., “Shallow-Water Bathymetry Estimation at Pantai Tok Jembal, Terengganu, Malaysia Using Landsat 8 (OLI),” *IOP Conference Series: Earth and Environmental Science*, vol. 767, p. 012008, 2021. *Crossref*, [http://doi.org/ 10.1088/1755-1315/767/1/012008](http://doi.org/10.1088/1755-1315/767/1/012008).
- [18] Ivan Henrico, “Optimal Interpolation Method to Predict the Bathymetry of Saldanha Bay,” *Transactions in GIS*, vol. 25, pp. 1991–2009, 2021. *Crossref*, <https://doi.org/10.1111/tgis.12783>
- [19] International Hydrographic Organization (IHO), IHO Standards for Hydrographic Surveys (S-44), 2020. [Online]. Available: https://iho.int/uploads/user/pubs/standards/s-44/s-44_edition_6.0.0_en.pdf
- [20] K. Kabiria, “Discovering Optimum Method to Extract Depth Information for Nearshore Coastal Waters From Sentinel-2a Imagery-Case Study: Nayband Bay, Iran,” *The International Archives of the Photogrammetry, Remote Sensing and Spatial Information Sciences*, vol. 42, no. 4, pp. 105–110, 2017. *Crossref*, <http://dx.doi.org/10.5194/isprs-archives-XLII-4-W4-105-2017>
- [21] M. F. O. Khattab et al., “Generate Reservoir Depths Mapping Using Digital Elevation Model: A Case Study of Mosul Dam Lake, Northern Iraq,” *Advances in Remote Sensing*, vol. 6, pp. 161 – 174, 2017. *Crossref*, <http://dx.doi.org/10.5194/isprs-archives-XLII-4-W4-105-2017>
- [22] Nadeeka Kumari, Kazuhito Sakai, and M.H.J.P. Gunarathna, “Are Geostatistical Interpolation Techniques Better Than Deterministic Interpolation Methods? A Study in Ulagalla Tank Cascade, Sri Lanka,” *In Proceedings PAWEEA-INWEPF International Conference Nara*, pp. 698-707, 2018.
- [23] Dulce Mata, Jose Úbeda, and Adrián Fernández-Sánchez, “Modelling of the Reef Benthic Habitat Distribution Within the Cabrera National Park (Western Mediterranean Sea),” *Annals of GIS*, vol. 27, no. 3, pp. 285-298, 2021. *Crossref*, <https://doi.org/10.1080/19475683.2021.1936169>
- [24] Mahrokh Moknatian et al., “Gonzalez, Development of Digital Bathymetry Maps for Lakes Azuei and Enriquillo Using Sonar and Remote Sensing Techniques,” *Transactions in GIS*, vol. 23, pp. 841–859, 2019. *Crossref*, <https://doi.org/10.1111/tgis.12532>
- [25] NOAA Coastal Services Center Tutorial: Benthic Terrain Modeler for Arcgis 10.1. National Oceanic and Atmospheric Administration (NOAA) Website, 2013. [Online]. Available: <https://coast.noaa.gov/data/digitalcoast/pdf/btm-tutorial.pdf>
- [26] Claudio Parente, and Andrea Vallario, “Interpolation of Single Beam Echo Sounder Data for 3d Bathymetric Model,” *International Journal of Advanced Computer Science and Applications*, vol. 10, no. 10, pp. 6-13, 2019. *Crossref*, <https://dx.doi.org/10.14569/IJACSA.2019.0101002>
- [27] R. R. Rodriguez, “Integration of Topographic and Bathymetric Digital Elevation Model Using Arcgis Interpolation Methods: A Case Study of the Klamath River Estuary,” Master’s Theses, University of Southern California, p.139, 2015. [Online]. Available: <https://spatial.usc.edu/wp-content/uploads/formidable/12/rachel-rodriguez.pdf>.
- [28] S. Saha, P. D. Kunte, and M. Kotha, Application of the Remote Sensing and Geo-Spatial Technology in Terrain Analysis and Terrain Classification in Context of Creation of SDI for Marine & Coastal Regions, 2016. [Online]. Available: <http://gsdiassociation.org/images/gsdi15/refereed/211-183.pdf>.
- [29] Curt D. Storlazzi et al., “End of the Chain? Rugosity and Fine-Scale Bathymetry from Existing Underwater Digital Imagery Using Structure-From-Motion (SFM) Technology,” *Coral Reefs*, vol. 35, no.3, pp. 889-894, 2016. *Crossref*, <https://doi.org/10.1007/s00338-016-1462-8>
- [30] TarlanSubarno et al., “Modeling Complex Terrain of Reef Geomorphological Structures in Harapan-Kelapa Island, Seribu Islands,” *Procedia Environmental Sciences*, vol. 33, pp. 478 – 486, 2016. *Crossref*, <https://doi.org/10.1016/j.proenv.2016.03.100>
- [31] I. B. Udoh, A. U. Ekpa, and D. A. Ndiyo, “Channel Maintenance Through Effective Utilization of Bathymetric Information,” *Journal of Environmental Design (JED)*, vol. 15, no. 2, pp.178 – 85, 2020.
- [32] I. B. Udoh and A. U. Ekpa, “Tidal Constants Derivation for Imo River,” *Nigerian Journal of Environmental Sciences and Technology (NIJEST)*, vol. 6, no. 1, pp. 139 – 148, 2022. *Crossref*, <https://doi.org/10.36263/nijest.2022.01.0335>
- [33] Shaun Walbridge et al., “Unified Geomorphological Analysis Workflows with Benthic Terrain Modeler,” *Geosciences*, vol. 8, no. 94, pp. 1-24, 2018. *Crossref*, <https://doi.org/10.3390/geosciences8030094>
- [34] Margaret F. J. Wilson et al., “Multiscale Terrain Analysis of Multibeam Bathymetry Data for Habitat Mapping on the Continental Slope,” *Marine Geodesy*, vol. 30, no. 1-2, pp. 3–35, 2007. *Crossref*, <https://doi.org/10.1080/01490410701295962>
- [35] Chia-Yu Wu et al., “Comparison of Different Spatial Interpolation Methods for Historical Hydrographic Data of the Lowermost Mississippi River,” *Annals of GIS*, vol. 25, no. 2, pp. 133-151, 2019. *Crossref*, <https://doi.org/10.1080/19475683.2019.1588781>
- [36] R. Mueller, “Utilizing Geographic Information Science Advancements for Bathymetric Mapping and Dredging Assessment of a Small Urban Lake in Southeastern Minnesota,” Saint Mary’s University of Minnesota, Winona (MN) Master’s Thesis, 2006.
- [37] Sarah Rosenthal, “Using GIS to Explore the Tradeoffs in Hydrographic Survey Planning: an Investigation of Sampling, Interpolation, and Local Geomorphology,” University of Southern California, Master’s Thesis, 2020.